Effect of heat treatments on the microstructures and tensile properties of an ultrafine-grained Al-Zn-Mg alloy processed by ECAP

Mohamed A. Afifi[a], Ying Chun Wang[a,b *], Pedro Henrique R. Pereira[c], Yi Huang[c], Yangwei Wang[a,b], Xingwang Cheng[a,b], Shukui Li[a,b], Terence G. Langdon[c]

[a]School of Materials Science and Engineering, Beijing Institute of Technology, Beijing 100081, China
[b]National Key Laboratory of Science and Technology on Materials under Shock and Impact, Beijing 100081, China
[c]Materials Research Group, Faculty of Engineering and the Environment, University of Southampton, SouthamptonSO17 1BJ, UK
*Corresponding author: Ying Chun Wang, e-mail: wangyc@bit.edu.cn; Tel: +861068913937 ext.801

Abstract

An investigation was conducted to determine the microstructures and tensile properties of an ultrafine-grained (UFG)Al-Zn-Mg alloy which was processed by equal-channel angular pressing (ECAP) for 1 and 4 passes at 423 K followed by heat treatments at 393 K for 5 or 20 h. Prior to ECAP, the Al alloy was in a T6 condition (solid solution treatment and peak aging) such that the precipitates introduced were able to hinder dislocation motions and enhance the grain refinement during ECAP. The results show that the yield strengths are enhanced but the ductilities are reduced after processing by ECAP for 1 and 4 passes but heat treatments at 393 K for up to 20 h are advantageous for improving both the yield strengths and the ductilities of the ECAP-processed alloy. The strength also increases with increasing holding time at 393 K from 5 to 20 h. A post-ECAP heat treatment improves the yield strength for the alloy after 1 pass of ECAP more effectively than after 4 passes. After post-ECAP heat treatments, precipitates containing GP zones, η', η, T and E are distributed within the Al matrix. Large numbers of uniformly distributed nano-scale fine precipitates of η', combined with ultra-fine grains and a high density of dislocations, contribute to produce an optimized balance between strength and ductility after ECAP for 1 pass and heat treatment at 393 K for 20 h.

Keywords: Al-Zn-Mg alloy; equal-channel angular pressing (ECAP); post-ECAP heat treatment; precipitates; tensile properties

1. Introduction

Age-hardenable 7000-series alloys, Al-Zn-Mg-(Cu), are used extensively in the aerospace, automobile and construction industries as they possess high strength to density ratios together with good fracture toughness [1,2]. In these precipitation-strengthened Al alloys, many small and uniformly distributed precipitates, mainly of GP zones and η', act as obstacles to dislocation motion and thereby strengthen the materials [3-5]. Nevertheless, there remains much interest in further improving their mechanical behavior. An effective approach for enhancing the properties is to develop Al alloys with ultrafine-grained (UFG) microstructures through the application of severe plastic deformation (SPD) processes such as equal-channel angular pressing (ECAP) [6,7]. However, materials processed by ECAP generally exhibit improved strength but only limited ductility at ambient temperature [8-10].

Several reports suggest that further improved properties may be achieved in Al alloys through post-ECAP heat treatments [11-17]. In some experimental conditions, enhanced strength and improved ductility can be achieved simultaneously by a combination of ECAP processing with appropriate post-ECAP heat treatments [13-17]. For example, the ultimate strength of a 7050 alloy was ~150 MPa higher than in conventional 7050 alloys with a good ductility of ~ 15% elongation after ECAP processing for 5 passes and post-ECAP heating at 393 K for 16 h [16]. These enhanced mechanical properties were attributed to the fine grains, high density of dislocations and the fine precipitates homogeneously distributed in the UFG matrix produced by the post-ECAP annealing. Another study examined the effect of heat treatment on the tensile properties of a 7075 alloy before and after ECAP and the results showed the yield strength increased by 120% after 1 pass of ECAP and there was an additional increase in strength by 7% together with a ductility improvement after a combination of 1 pass of ECAP and post-ECAP

aging at 373 K for 30 h [17]. Very limited information is available to date on the influence of post-ECAP heat treatments on the mechanical properties and microstructures of Al-Zn-Mg alloys but nevertheless the available data suggest that only an appropriate post-ECAP heat treatment provides both improved strength and ductility [16-18]. For example, a 7075 alloy was processed by ECAP for 1-3 passes at 393 K followed by heat treatments at 393 K for different times and the peak microhardness values were achieved after aging treatments of 9 h after 1 and 2 ECAP passes but only 6 h after 3 ECAP passes due to the increased volume fraction of η' [18].

A review of the available data shows that an optimization of strength and ductility may be achieved in 7000-series Al alloys through processing by ECAP and then aging in the post-ECAP condition [11-13,17-21] but information is not available on the effect of post-ECAP heat treatments on the microstructure and tensile properties of an alloy subjected to initial precipitation-strengthening by a T6 treatment (solid solution treatment and peak aging) prior to ECAP. Accordingly, this research was initiated to examine whether further microstructural evolution and improvements in tensile properties may be achieved by processing by ECAP and using post-ECAP heat treatments in an alloy initially precipitation-strengthened with a T6 treatment.

2. Experimental material and procedures

The experiments were conducted using an Al-Zn-Mg alloy having a chemical composition, in wt. %, of Al-4.53 Zn-2.52Mg-0.35Mn-0.2Cr-0.11Cu-0.1Zr which was received in a T6 state after solution treating at 743 K for 1 h and further aging at 393 K for 24 h. Billets of the as-received material with diameters of 9.8 mm and lengths of 65 mm were processed by either 1 or 4 ECAP passes using a solid die having an internal channel angle of 90° and an outer arc of curvature of 20° without a back-pressure. These angular values impose an equivalent strain of ~1

in each pass [22] and the ECAP processing was performed at 423 K with a deformation speed of 2 mm/s using route B_c where the billet is rotated by 90° in the same sense between each pass. ECAP samples were heated in the die entry channel for 5 minutes homogenization before pressing. A Crown anti-seize compound 9105 was used as a lubricant to reduce the friction between the die and the sample.

Following ECAP, samples were subjected to heat treatments at 393 K for 5 or 20 h using a forced convection furnace and then cooled in air. For convenience, the sample nomenclatures are presented in Table 1 together with the corresponding processing parameters.

The tensile testing was carried out at room temperature (~298 K) at an initial strain rate of 1.0×10^{-3} s^{-1}using an Instron testing machine with the strain and strain rate measured using optical sensors. Planar dog-bone tensile samples were machined with nominal gauge dimensions of $10 \times 2 \times 1.3$ mm^3 and polished with a finishing grit of grade 2000 SiC paper to remove any defects before testing. At least two samples were tested for each condition to verify reproducibility. The microstructures were characterized by transmission electron microscopy (TEM) using an F20 Field Emission microscope operating at 200 kV. Samples for TEM were prepared by mechanical grinding using grit papers with different particle sizes ranging from 1000 to 5000 mesh followed by thinning to electron transparency using a Gatan Dual Ion Milling System.

3. Experimental results

3.1 Tensile behavior

The tensile true stress-true strain curves for the as-received, the ECAP-processed and the post-ECAP heat-treated Al-Zn-Mg alloy are shown in Fig.1 and the main tensile properties

derived from these curves with standard deviations are summarized in Table 2. These results reveal that the as-received material has the lowest yield strength but the highest ultimate strength due to its superior work hardening capability and good ductility. After ECAP processing for 1 pass, the yield strength increases but the ductility is notable reduced. Increasing to 4 passes, the yield strength further increases and also the ductility increases.

Post-ECAP heat treatments are advantageous for improving both the yield strength and the ductility of the ECAP-processed alloy as also shown in Fig.1. It is apparent that sample 1P-20 exhibits excellent tensile properties with the highest yield strength among all processing conditions together with improved ductility. The yield and the ultimate strengths for this condition are ~376 MPa and ~440 MPa, respectively, and the elongation is ~17%. The strength of sample 1P-5 is close to 1P-20 but the elongation is only ~14%. By comparison with the samples 4P, 4P-5 and 4P-20, 1P-20 also has higher yield and ultimate strength. In addition, a comparison of the strengths of 1P-5 and 1P-20 with 4P-5 and 4P-20 reveals that the heat treatments at 393 K for up to 20 h improve the strengths of the alloy more effectively after 1 pass than after 4 passes. Finally, it is reasonable to conclude from Fig. 1 that sample 1P-20 exhibits an optimized balance between strength and ductility in this alloy.

3.2 Microstructural characteristics

The microstructures of the as-received alloy and the alloy after processing by ECAP for 1 and 4 passes were examined and characterized in earlier reports [23, 24]. These results showed the microstructure after 1 pass of ECAP was an elongated dislocation cell structure with a few platelet precipitates of ~120 nm and numerous fine spherical precipitates including some GP zones as well as η' and a few η phases. After further processing to 4 passes, the microstructure

displayed equiaxed grains having a size of ~200 nm distributed with predominantly η' and η phases and some limited retained GP zones. The precipitates introduced prior to ECAP by the T6 treatment can speed up the grain refinement during ECAP and increase the dislocation density by pinning dislocations [25-27].

For the present research, typical micrographs of the alloy processed by post-ECAP heat treatments are shown in Fig. 2. Inspection of Fig. 2(a) shows the microstructure of the 1P-5 sample has nearly equiaxed grains which evolved from the elongated dislocation cell structure after ECAP processing for 1pass [23]. It is apparent that the evolution is incomplete after post-heating at 393 K for 5 h because the elongated boundaries are not well-defined. Also, many dislocations and dislocation tangles are present in Fig.2(a). Increasing the holding time at 393 K to 20 h, Fig. 2(b) shows that the microstructure is now well-defined with reasonably equiaxed grains having an average size of ~870nm and with dislocations within some grains. Figures 2(c) and (d) show the microstructures of the 4P-5 and 4P-20 samples, respectively, where the grain sizes are not significantly changed by the heat treatments by comparison with the grain size of ~200 nm reported earlier for the 4P sample [23, 24]. Nevertheless, a high density of dislocations and dislocation tangles are visible within the grains of the 4P-5 and 4P-20 samples.

Figure 3 displays characteristics of the precipitates in the post-ECAP heat-treated samples where Fig. 3(a) shows fine precipitates homogeneously distributed within the grains as well as precipitate free zones (PFZ) of ~100 nm in width lying along the grain boundaries (GB) of the1P-5 sample. The inserted selected area electron diffraction (SAED) pattern along $<112>_{Al}$ shows that the major precipitates in 1P-5 are η' and GP zones with the presence of weak spots of Al_3Zr. In addition, T ($Al_{20}Mn_3Cu_2$) and E ($Al_{18}Mg_3Cr_2$) phases were also detected at $\{152\}_{Al}$ and $\{111\}_{Al}$, respectively [28]. The size of the spherical precipitates within the grains is in the range

of ~8-50 nm while a few plate-like precipitates, mainly distributed along the grain boundaries, have average lengths of ~90 nm.

Diffraction along $<111>_{Al}$ in Fig. 3(b) shows that the main precipitates in the microstructure of the 1P-20 sample are η' along $\{011\}_{Al}$, $\{201\}_{Al}$, $\{202\}_{Al}$ and $\{402\}_{Al}$ while several spots of η along $\{110\}_{Al}$ are also observed [29,30]. In addition, the T phase along $\{013\}_{Al}$ and E phase along $\{133\}_{Al}$ are also present. The number fractions of both fine spherical precipitates with diameters varying from ~4 to 60 nm and limited number of plate-like precipitates with mean lengths of ~90 nm increases significantly in the 1P-20 sample compared with the material aged for 5 h. The high resolution transmission electron microscopy (HRTEM) image inserted in Fig.3(b) displays large numbers of fine spherical η' precipitates which are homogeneously distributed in the Al matrix

Precipitates of η' and η with spots of GP zones are shown in Fig. 3(c) in the 4P-5 sample along $<110>_{Al}$. In addition, reflections of E phase along $\{117\}_{Al}$, T phase along $\{113\}_{Al}$ and Al_3Zr dispersoids along $\{100\}_{Al}$ are evident through the SAED patterns. The 4P-5 sample has a large number fraction of uniformly distributed spherical precipitates with diameters ranging from ~10 to ~75 nm with a few coarser platelet precipitates with lengths of ~100 nm along dislocations and grain boundaries. By comparison with the 4P sample described earlier [23, 24], the numbers of precipitates have increased slightly with limited precipitate growth. Diffraction along $<110>_{Al}$ in Fig. 3(d) shows precipitates in the Al matrix mainly of η along $\{111\}_{Al}$, $\{122\}_{Al}$ and $\{112\}_{Al}$ with some η' along $\{135\}_{Al}$ and Al_3Zr dispersoids along $\{110\}_{Al}$ [29,31-35]. Furthermore, the E phase has spots along $\{123\}_{Al}$ and the T phase along $\{113\}_{Al}$. By comparison with the 4P-5 sample, 4P-20 has larger quantities of finer precipitates with sizes ranging from ~6-75 nm uniformly distributed in the matrix and with an increase in the numbers of platelets

and lath-like precipitates with average lengths of ~120 nm lying along grain boundaries and dislocations. Two η' and one η parallel to (440), which is being nucleated from η' parallel to (224), can be observed in the HRTEM image inserted in Fig.3(d). Comparing Fig 3(d) with the HRTEM micrograph in Fig 3(b), it is apparent that the numbers of fine η' precipitates in the matrix of the 4P-20 sample are lower than in the 1P-20 sample.

A grain boundary precipitation of platelet phases in the 1P-5 sample is visible in Fig. 4(a) with fine spherical precipitates within the grains separated by a PFZ having a width of ~ 100 nm. The formation of a PFZ is generally attributed to either vacancy depletion or solute depletion. Thus, vacancy depletion takes into account the effects of vacancy sinks which lead to retarded precipitation around the grain boundaries compared with the grain interiors [36] whereas, by contrast, solute depletion takes into account the depleted solute concentrations near the grain boundaries [37]. Furthermore, the precipitates are predominantly η' at $\{111\}_{Al}$ with weak spots of η along $\{111\}_{Al}$ as displayed by the SAED pattern along $<112>_{Al}$ inserted in Fig.4(a) [28, 30]. The η' phases of ~45 nm in length exhibit plate-like morphology nucleated along the grain boundaries in the 1P-5 sample as shown in Fig. 4(b). Furthermore, the PFZ almost disappears after increasing the heating time to 20 h as shown in Fig.3(b) because the longer holding time permits the diffusion of solutes in the grain boundary area and they eventually precipitate during the heat treatment [38].

Much overlapping of larger precipitates may be observed in Fig.3 and for a more detailed assessment of these features the HRTEM images in Fig. 5 contain overlapping precipitates. Two spherical overlapped E phases and two oval T phases are visible in Fig. 5(a) and 5(b), respectively, for the alloy processed by 1 ECAP pass and further aged at 393 K for 20 h. The overlapping of two E phases in the 4P-20 sample is shown in Fig. 5 (c) where one is spherical

and the other is a platelet having different orientations as verified by the Fast Fourier Transform (FFT) patterns. The overlapping of two platelet T phases having similar orientations identified by the corresponding FFT is given in Fig. 5(d). Inspection of Figs.3(a)-(d) reveals that there is more overlapping of precipitates with increasing heating time from 5 to 20 h and it is reasonable to assume that the overlapping is due to the growing together of adjacent precipitates of the T and E phases.

4. Discussion

4.1 The strengthening after ECAP processing

In order to understand the contributions of different mechanisms to the strength of Al-Zn-Mg alloys, it is necessary to examine separately several different strengthening processes. These mechanisms are (i) work-hardening due to the interactions of dislocations, (ii) grain boundary strengthening, (iii) solid solution hardening and (iv) precipitation strengthening [39-42] In practice, the influence of solid solution strengthening may be neglected because the Al alloy was subjected to an aging heat treatment (T6) before the ECAP processing [40].

In earlier research it was shown that ECAP processing leads to successful refinement of the coarse grains into ultrafine grains with the presence of a high density of dislocations within these grains [23]. Consequently, following the Hall-Petch relationship [43], it was demonstrated that grain refinement through ECAP processing was the major contributor to the high yield strength [43, 44]. However, due to dislocation tangles and networks within the grains which impede dislocation motion [11], the large numbers of dislocations in the 1P and 4P samples are expected to make a significant contribution to the strength enhancement of the ECAP-processed alloy. In addition, precipitates may obstruct dislocation motion by either the Orowan bypass or shearing

mechanisms [40]. During ECAP, the results show that the precipitates in the as-received material with sizes of ~120 nm are fragmented into fine spherical precipitates and this increases the overall fraction of precipitates in the alloy and leads to further strength enhancement [23].

4.2The strengthening after ECAP and post ECAP heat treatments

The results of tensile testing show that the post-ECAP heat treatments are very advantageous in improving both the yield strength and the ductility of the Al-Zn-Mg alloy. Different types of precipitates are present after the post-ECAP heat treatments at 393 K for 5-20 h and the results demonstrate that the combined effect of fine scale precipitation coupled with grain boundary strengthening increases the yield strength without significantly compromising the ductility. In addition, heating at 393 K produces a limited reduction in the numbers of dislocations and no concomitant grain growth. Thus, grain boundary strengthening and dislocation strengthening make contributions after the heat treatment and this contrasts with the ECAP-processed Al alloy. It is also the reason for the low work hardening rate in the post-ECAP heat treated materials.

The differences in strength after ECAP processing for different numbers of passes and subsequent post-ECAP heat treatments at 393 K for different times are attributed directly to precipitate evolution. Following Deschamps and Bréchet [45], if all precipitates are sheared the strength may be calculated using either Friedel statistics [46] or Kocks statistics [47] where

$$\sigma_P^F = \sqrt{\frac{3k^{\frac{3}{2}} M\mu}{4\Pi\beta\sqrt{b}}} (f_v R)^{1/2} \qquad (1)$$

and

$$\sigma_P^K = KM\mu\sqrt{\frac{3}{2\Pi}}f_v^{1/2} \quad (2)$$

whereas if all precipitates are by-passed the yield strength is then expressed by

$$\sigma_P^F = 0.7M\mu b\frac{f_v^{1/2}}{R} \quad (3)$$

or

$$\sigma_P^K = 0.6M\mu b\frac{f_v^{1/2}}{R} \quad (4)$$

where σ_P^F and σ_P^K are the yield strength increments using the Friedel and Kocks models, respectively, K is an adjustable parameter characteristic of the mechanism, β is a constant, M is the Taylor factor, μ is the matrix shear modulus, b is the Burger vector, f_v is the particle volume fraction and R is the mean radius.

According to equations (1)-(4), an increase in the volume fraction of fine precipitates will produce a further impediment to dislocation motion [39]. The results displayed in Fig.1 and Table 2 show that the strength of the 1P-5 sample is higher than for 1P and this is due to the increased volume fraction of fine precipitates where these are mainly GP zones and η' precipitates. Increasing the heating time to 20h for the 1P samples leads to a transformation of additional GP zones into ultrafine η' so that additional and finer precipitates of η' are present. The large numbers of semi-coherent nano-sized precipitates shown in Fig.3(b) increases the volume fraction, $f_{v,}$ and these precipitates pin the dislocations effectively leading to an improved strength [40,48]. Trapping dislocations by these fine precipitates also leads to a uniform elongation due to sustained work hardening and this gives an improvement in the overall ductility [49]. As a result,

the 1P-20 samples display the optimized balance between strength and ductility by comparison with all other samples.

Similar to the 1P-20 samples, increasing the heat treatment time of the 4P samples from 5 to 20 h leads to an increase in the numbers of fine precipitates and consequently to an enhanced strength compared to the 4P-5 sample. Nevertheless, inspection of Table 2 shows that the strength of the 4P-20 sample is slightly lower than the 1P-20 sample and this is attributed to a transformation of η' to η as the higher dislocation density and finer grains in the 4P sample accelerate this transformation during heating [23]. In addition, the platelet T and E phases observed after the post-ECAP heat treatments are incoherent with the Al matrix as verified by HRTEM so that the operative strengthening process is the Orowan bypass mechanism [40,50-51]. It is evident that these platelet precipitates are coarser in size and display a low volume fraction, as shown in Fig. 3. Therefore, based on equations (3) and (4), it is estimated that the strength increment from dislocation bypassing from platelet precipitates makes only a small contribution to the strengthening of the material after the post-ECAP heat treatments.

As already noted, PFZ may be formed by vacancy or solute depletion and the presence of coarse η' precipitates along the grain boundaries in Fig. 4 are attributed to a decreased saturation of solute atoms [37,52-53]. Therefore, the main mechanism of PFZ formation in the 1P-5 sample is from solute depletion near the grain boundaries. Increasing the numbers of ECAP passes leads to an increase in solute segregation at boundaries [53] but there is no evidence for PFZ near the grain boundaries in the 4P-5 samples. The PFZ has a size of ~100 nm in the 1P-5 sample and this may decrease the elongation of the material because these zones are relatively softer than the matrix and easily form preferential deformation areas which ultimately lead to stress concentrations and premature failure along the grain boundaries [54]. Accordingly, the Al-Zn-

Mg alloy processed by 1 ECAP pass and further aged for 5 h at 393 K is less ductile by comparison with the same alloy subjected to other post-ECAP heat treatments such as aging at 393 K for 20 h.

5. Summary and conclusions

1. ECAP processing of an Al-Zn-Mg alloy for 1 and 4 passes effectively enhances the yield strength but the ductility is reduced. Post-ECAP heat treatments at 393K are advantageous in improving both the yield strength and the ductility and the experiments show that the yield strength increases when the holding time at 393K is increased from 5 to 20 h. Post-ECAP heat treatments under identical conditions improve the yield strength more effectively after 1 pass than after 4 passes. The alloy processed through 1 ECAP pass and further aged at 393 K for 20 h exhibits an optimized balance between strength and ductility.

2. Precipitates including GP zones, η', η, T and E were identified in the Al matrix after post-ECAP heat treatments. When the holding time at 393 K was increased from 5 to 20 h after 1 pass of ECAP, the precipitate-free zones near the grain boundaries were reduced significantly and there was precipitation of a large fraction of ultrafine η' and some η. After 4 passes, the number of fine η' and η precipitates increased together with the presence of coarse T and E phases.

3. It is concluded that large numbers of uniformly distributed nano-scale precipitates of η', combined with ultrafine grains and high dislocation densities, contribute to give the optimized combination of yield strength and ductility after 1 pass of ECAP and heat treatment at 393 K for 20 h.

Acknowledgements

This work was supported by the National Natural Science Foundation of China under Grants nos. 51671030, the Brazilian Federal Agency for the Support and Evaluation of Graduate Education (CAPES) and the European Research Council under ERC Grant Agreement no. 267464-SPDMETALS.

References

[1] M.E. Fine, Precipitation Hardening of Aluminum Alloys,Metall. Trans. A 6 (1975) 625–630. doi: 10.1007/BF02672283.

[2]M. Nakai, T.Eto, High strength heat treatable 7000 series aluminum alloy of excellent corrosion resistance and a method of producing thereof. United States: Kabushiki Kaisha Kobe Seiko Sho (Kobe,JP), US Patent 6048415, 2000.

[3] S.K. Maloney, K. Hono, I.J. Polmear, S.P. Ringer, The chemistry of precipitates in an aged Al-2.1Zn-1.7Mg at.% alloy, Scr. Mater. 41 (1999) 1031–1038. doi:10.1016/S1359-6462(99)00253-5.

[4] M. Liu, B. Klobes, K. Maier, On the age-hardening of an Al–Zn–Mg–Cu alloy : A vacancy perspective, Scr. Mater. 64 (2011) 21–24. doi:10.1016/j.scriptamat.2010.08.054.

[5] Y.L. Wu, F.H. Froes, A. Alvarez, C.G. Li, J. Liu, Microstructure and properties of a new super-high-strength Al–Zn–Mg–Cu alloy C912, Mater. Des.18 (1997) 211–215.doi: 10.1016/S0261-3069(97)00084-8.

[6] R.Z. Valiev, T.G. Langdon, Principles of equal-channel angular pressing as a processing tool for grain refinement, Prog. Mater. Sci. 51 (2006) 881-981. doi: 10.1016/j.pmatsci.2006.02.003.

[7] Y. T. Zhu, R.Z. Valiev, T.G. Langdon, N. Tsuji, K. Lu, Processing of nanostructured metals and alloys via plastic deformation, MRS Bull. 35 (2010) 977–981. doi:10.1557/mrs2010.702.

[8]R.Z. Valiev, I.V. Alexandrov, Y.T. Zhu, T.C. Lowe, Paradox of strength and ductility in metals processed by severe plastic deformation, J. Mater. Res. 17 (2002) 5-8. doi: 10.1557/JMR.2002.0002.

[9] R.Z.Valiev, Nanostructuring of metals by severe plastic deformation for advanced properties, Nat. Mater. 3 (2004) 511–516. doi:10.1038/nmat1180.

[10]C.C. Koch, Optimization of strength and ductility in nanocrystalline and ultrafine grained metals, Scr. Mater. 49 (2003) 657–662. doi:10.1016/S1359-6462(03)00394-4.

[11]W.J. Kim, J.K. Kim, T.Y. Park, S.I. Hong, D.I. Kim, Y.S. Kim, J.D. Lee, Enhancement of strength and superplasticity in a 6061 Al Alloy processed by equal-channel-angular-pressing, Metall. Mater. Trans. A 33 (2002) 3155–3164. doi:10.1007/s11661-002-0301-4.

[12] M.H.Goodarzy, H.Arabi, M.A.Boutorabi, S.H.Seyedein, S.H.Hasani Najafabadi, The effects of room temperature ECAP and subsequent aging on mechanical properties of 2024 Al alloy, J. Alloys Compd.585(2014) 753-759.doi:10.1016/j.jallcom.2013.09.202.

[13]M.H. Shaeri, M.T. Salehi, S.H. Seyyedein, M.R. Abutalebi, J.K. Park, Microstructure and mechanical properties of Al–7075 alloy processed by equal channel angular pressing combined with aging treatment, Mater. Des.57 (2014) 250–257. doi:10.1016/j.matdes.2014.01.008.

[14] W.J. Kim, C.S. Chung, D.S. Ma, S.I. Hong, H.K. Kim, Optimization of strength and ductility of 2024 Al by equal channel angular pressing (ECAP) and post-ECAP aging, Scr. Mater. 49 (2003) 333–338. doi:10.1016/S1359-6462(03)00260-4.

[15] L.J. Zheng, C.Q. Chen, T.T. Zhou, P.Y. Liu, M.G. Zeng, Structure and properties of ultrafine-grained Al-Zn-Mg-Cu and Al-Cu-Mg-Mn alloys fabricated by ECA pressing combined with thermal treatment, Mater. Charact.49 (2002) 455–461. doi:10.1016/S1044-5803(03)00069-X.

[16] L.J. Zheng, H.X. Li, M.F. Hashmi, C.Q. Chen, Y. Zhang, M.G. Zeng, Evolution of microstructure and strengthening of 7050 Al alloy by ECAP combined with heat-treatment, J. Mater. Process. Technol. 171 (2006) 100–107. doi:10.1016/j.jmatprotec.2005.06.049.

[17] W.J. Kim, J.K. Kim, H.K. Kim, J.W. Park, Y.H. Jeong, Effect of post equal-channel-angular-pressing aging on the modified 7075 Al alloy containing Sc, J. Alloys Compd. 450 (2008) 222–228. doi:10.1016/j.jallcom.2006.10.151.

[18] M.H. Shaeri, M. Shaeri, M.T. Salehi, S.H. Seyyedein, M.R. Abutalebi, Effect of equal channel angular pressing on aging treatment of Al-7075 alloy, Prog. Nat. Sci. Mater. Int. 25 (2015) 159–168. doi:10.1016/j.pnsc.2015.03.005.

[19] M. Hockauf, L.W. Meyer, B. Zillmann, M. Hietschold, S. Schulze, L. Krüger, Simultaneous improvement of strength and ductility of Al–Mg–Si alloys by combining equal-channel angular extrusion with subsequent high-temperature short-time aging, Mater. Sci. Eng. A503 (2009) 167–171. doi:10.1016/j.msea.2008.02.051.

[20] W.J. Kim, J.Y. Wang, Microstructure of the post-ECAP aging processed 6061 Al alloys, Mater. Sci. Eng. A464 (2007) 23–27. doi:10.1016/j.msea.2007.03.074.

[21] G. Tan, Y.E. Kalay, C.H. Gür, Long-term thermal stability of Equal Channel Angular Pressed 2024 aluminum alloy, Mater. Sci. Eng. A. 677 (2016) 307–315. doi:10.1016/j.msea.2016.09.048.

[22]Y. Iwahashi, J. Wang, Z. Horita, M. Nemoto, T.G. Langdon, Principle of equal-channel angular pressing for the processing of ultra-fine grained materials, Scripta Mater. 35 (1996) 143–146. doi:10.1016/1359-6462(96)00107-8.

[23] M.A. Afifi, P.H.R. Pereira, Y.C. Wang, Y. Wang, S. Li, T.G. Langdon, Effect of ECAP processing on microstructure evolution and dynamic compressive behavior at different temperatures in an Al-Zn-Mg alloy, Mater. Sci. Eng. A684 (2017) 617–625. doi:10.1016/j.msea.2016.12.099.

[24] M.A. Afifi, Y.C. Wang, P.H.R. Pereira, Y. Wang, S. Li, Y. Huang, T.G. Langdon, Characterization of precipitates in an Al-Zn-Mg alloy processed by ECAP and subsequent annealing, Mater. Sci. Eng. A. 712 (2018) 146–156. doi:10.1016/j.msea.2017.11.091.

[25] C.M. Cepeda-Jiménez, J.M. García-Infanta, E.F. Rauch, J.J. Blandin, O.A. Ruano, F. Carreño, Influence of processing severity during equal-channel angular pressing on the microstructure of an Al-Zn-Mg-Cu alloy, Metall. Mater. Trans. A 43 (2012) 4224–4236. doi:10.1007/s11661-012-1206-5.

[26] S. Fritsch, M. Scholze, M.F.-X. Wagner, Cryogenic forming of AA7075 by equal-channel angular pressing, Mat.-wiss. u.Werkstofftech. 43 (2012) 561–566. doi:10.1002/mawe.201200001.

[27] S. Fritsch, M.F. -X. Wagner, On the Effect of Natural Aging Prior to Low Temperature ECAP of a High-Strength Aluminum Alloy, Metals. 8 (2018) 1–10. doi:10.3390/met8010063.

[28] W. B. Pearson, A Handbook of Lattice Spacings and Structures of Metals and Alloys, Pergamon Press, Oxford, 1958.

[29] G. Sha, Y.B. Wang, X.Z. Liao, Z.C. Duan, S.P. Ringer, T.G. Langdon, Influence of equal-channel angular pressing on precipitation in an Al–Zn–Mg–Cu alloy, Acta Mater. 57 (2009) 3123–3132. doi:10.1016/j.actamat.2009.03.017.

[30] A. Kverneland, V. Hansen, R. Vincent, K. Gjønnes, J. Gjønnes, Structure analysis of embedded nano-sized particles by precession electron diffraction η'-precipitate in an Al–Zn–Mg alloy as example, Ultramicros. 106 (2006) 492–502. doi:10.1016/j.ultramic.2006.01.009.

[31] X.Z. Li, V. Hansen, J. GjØnnes, L.R. Wallenberg, HREM study and structure modeling of the η' phase, the hardening precipitates in commercial Al–Zn–Mg alloys, Acta Mater. 47 (1999) 2651–2659. doi:10.1016/S1359-6454(99)00138-X.

[32] L.K. Berg, J. Gjønnes, V. Hansen, X. Z. Li, M. K. -Wedel, G. Waterloo, D. Schryvers, L.R. Wallenberg, GP-zones in Al–Zn–Mg alloys and their role in artificial aging, Acta Mater. 49 (2001) 3443–3451. doi: 10.1016/S1359-6454(01)00251-8.

[33] A. Deschamps, Y. Bréchet, Influence of quench and heating rates on the ageing response of an Al–Zn–Mg–(Zr) alloy, Mater. Sci. Eng. A251 (1998) 200–207. doi:10.1016/S0921-5093(98)00615-7.

[34] H. Löffler, I. Kovacs, J. Lendvai, Review: Decomposition processes in AI-Zn-Mg alloys, J. Mater. Sci. 18 (1983) 2215–2240. doi:10.1007/BF00541825.

[35] J. Gjønnes, C.J. Simensen, An electron microscope investigation of the microstructure in an aluminium-zinc-magnesium alloy, Acta Metall. 18 (1970) 881–890. doi:10.1016/0001-6160(70)90016-7.

[36] J. D. Embury, R. B. Nicholson, The nucleation of precipitates: the system Al-Zn-Mg, Acta Metall.13 (1965) 403–417.doi: 10.1016/0001-6160(65)90067-2.

[37] C.R. Shastry, G. Judd, A Study of grain boundary precipitate-free zone formation in an AI-Zn-Mg alloy, Metall. Trans. 2 (1971) 3283–3287.doi: 10.1007/BF02811608.

[38] Y.Q. Chen, S.P. Pan, S.W. Tang, W.H. Liu, C.P. Tang, F.Y. Xu, Formation mechanisms and evolution of precipitate-free zones at grain boundaries in an Al–Cu–Mg–Mn alloy during homogenisation,J. Mater. Sci. 51 (2016) 7780–7792. doi:10.1007/s10853-016-0062-x.

[39] J. Gubicza, I. Schiller, N.Q. Chinh, J. Illy, Z. Horita, T.G. Langdon, The effect of severe plastic deformation on precipitation in supersaturated Al–Zn–Mg alloys, Mater. Sci. Eng.A 460–461 (2007) 77–85. doi:10.1016/j.msea.2007.01.001.

[40] K. Ma, H. Wen, T. Hu, T.D. Topping, D. Isheim, D.N. Seidman, E.J. Lavernia, J.M. Schoenung, Mechanical behavior and strengthening mechanisms in ultrafine grain precipitation-strengthened aluminum alloy, Acta Mater. 62 (2014) 141–155. doi: 10.1016/j.actamat.2013.09.042.

[41] K.L. Kendig, D.B. Miracle, Strengthening mechanisms of an Al-Mg-Sc-Zr alloy, Acta Mater. 50 (2002) 4165–4175. doi:10.1016/S1359-6454(02)00258-6.

[42] M. Cabibbo, Microstructure strengthening mechanisms in different equal channel angular pressed aluminum alloys, Mater. Sci. Eng. A. 560 (2013) 413–432. doi:10.1016/j.msea.2012.09.086.

[43] P.H.R. Pereira, Y. C. Wang, Y. Huang, T. G. Langdon, Influence of grain size on the flow properties of an Al-Mg-Sc alloy over seven orders of magnitude of strain rate, Mater. Sci. Eng. A 685 (2017) 367–376.doi:10.1016/j.msea.2017.01.020.

[44] E.N. Hahn, M.A. Meyers, Grain-size dependent mechanical behavior of nanocrystalline metals, Mater. Sci. Eng. A. 646 (2015) 101–134. doi:10.1016/j.msea.2015.07.075.

[45] A. Deschamps, Y. Bréchet, Influence of predeformation and ageing of an Al–Zn–Mg alloy–II. modeling of precipitation kinetics and yield stress, Acta Mater.47(1998)293–305.doi:10.1016/S1359-6454(98)00296-1.

[46] J. Friedel, Dislocations, Pergamon Press, Oxford, 1964.

[47] U.F. Kocks, A statistical theory of flow stress and work-hardening, Philos. Mag. 13 (1966) 541–566. doi:10.1080/14786436608212647.

[48] S. Zhang, W. Hu, R. Berghammer, G. Gottstein, Microstructure evolution and deformation behavior of ultrafine-grained Al-Zn-Mg alloys with fine η' precipitates, Acta Mater. 58 (2010) 6695–6705. doi:10.1016/j.actamat.2010.08.034.

[49]S. Cheng, Y. H. Zhao, Y. T. Zhu, E. Ma, Optimizing the strength and ductility of fine structured 2024 Al alloy by nano-precipitation, Acta Mater. 55 (2007) 5822–5832. doi:10.1016/j.actamat.2007.06.043.

[50] A. Simar, Y. Bréchet,B.deMeester, A.Denquin, T.Pardoen, Sequential modeling of local precipitation, strength and strain hardening in friction stir welds of an aluminum alloy 6005A-T6, Acta Mater. 55 (2007) 6133–6143. doi:10.1016/j.actamat.2007.07.012.

[51] G. Fribourg, Y. Bréchet,A. Deschamps, A. Simar, Microstructure-based modelling of isotropic and kinematic strain hardening in a precipitation-hardened aluminium alloy, Acta Mater.59 (2011) 3621–3635. doi:10.1016/j.actamat.2011.02.035.

[52]E.A. Starke, The causes and effects of “denuded” or “precipitate-free” zones at grain boundaries in aluminum-base alloys, JOM 22(1)(1970)54–63.doi:10.1007/BF03355628.

[53] G. Sha, L. Yao, X. Liao, S.P. Ringer, Z. C. Duan, T.G. Langdon, Segregation of solute elements at grain boundaries in an ultrafine grained Al–Zn–Mg– Cu alloy, Ultramicros.111 (2011) 500–505. doi:10.1016/j.ultramic.2010.11.013.

[54] D.S. Park, S.W. Nam, Effect of precipitate free zones on low cycle fatigue life of AI–Zn–Mg alloy, Mater.Sci. Technol. 11 (1995) 921–925.doi:10.1179/mst.1995.11.9.921.

Figure Captions

Fig. 1 True stress-true strain curves of the as-received Al-Zn-Mg alloy, ECAP processed at 423K and post-ECAP heat treated at 393K for 5 or 20h.

Fig. 2 Typical TEM micrographs of Al-Zn-Mg alloy along $<001>_{Al}$ zone axis processed by ECAP for 1 pass followed by heat treatments at 393K for (a) 5h, (b) 20h, and by ECAP for 4 passes followed by heat treatments at 393K for (c) 5h and (d) 20h.

Fig. 3 Typical TEM micrographs and corresponding SAED of Al-Zn-Mg alloy processed by ECAP for 1 pass followed by heat treatments at 393K for (a) 5h, (b) 20h, and by ECAP for 4 passes followed by heat treatments at 393K for (c) 5h and (d) 20h.

Fig. 4 TEM Micrographs of the Al-Zn-Mg alloy after ECAP for 1 pass and post-ECAP heat treatment at 393K for 5h:(a) TEM image showing PFZ and precipitates along the grain boundary with corresponding SAED along $<112>_{Al}$ and (b) HRTEM image of a plate-like η' phase along the grain boundaries.

Fig. 5 HRTEM images of different phases in the Al-Zn-Mg alloy after ECAP for 1pass followed by heat treatment at 393K for 20h showing overlapping of (a) two spherical E phases, (b) two spherical T phases, and after ECAP for 4 passes followed by heat treatment at 393K for 20h showing overlapping (c) one spherical with one platelet E phase and (d) two platelets T phases.

Table Captions

Tab.1.Sample designation of Al-Zn-Mg alloyand their corresponding processing parameters.

Tab.2. Tensile property data of the Al-Zn-Mg alloy after different processing conditions.

Table

Tab.1. Sample designation of Al-Zn-Mg alloy and their corresponding processing parameters.

Sample	Processing condition
As-received	Solid solution treatment at 743 K for 1 h and then aging at 393 K for 24 h
1P	ECAP processing for 1 pass
4P	ECAP processing for 4 passes
1P-5	ECAP processing for 1 pass and subsequent heat treatment at 393 K for 5 h
1P-20	ECAP processing for 1 pass and subsequent heat treatment at 393 K for 20 h
4P-5	ECAP processing for 4 passes and subsequent heat treatment at 393 K for 5 h
4P-20	ECAP processing for 4 passes and subsequent heat treatment at 393 K for 20 h

Table

Tab.2. Tensile property data of the Al-Zn-Mg alloy after different processing conditions.

Sample	σ_{yield} (MPa)	$\sigma_{ultimate}$ (MPa)	True fracture strain (%)	Elongation (%)
As-received	281±1.2	485±1.2	18±0.2	20±0.2
1P	314±2	385±2.5	7±0.7	7±0.6
4P	347±1.9	390±1.8	11±0.2	12±0.2
1P-5	373±2.5	421±2.8	13±1	14±1
4P-5	344±1.8	400±2.1	16±0.9	17±0.9
1P-20	376±2	440±2.3	16±0.5	17±0.7
4P-20	362±2.8	414±2.7	16±0.1	17±0.1

Figure

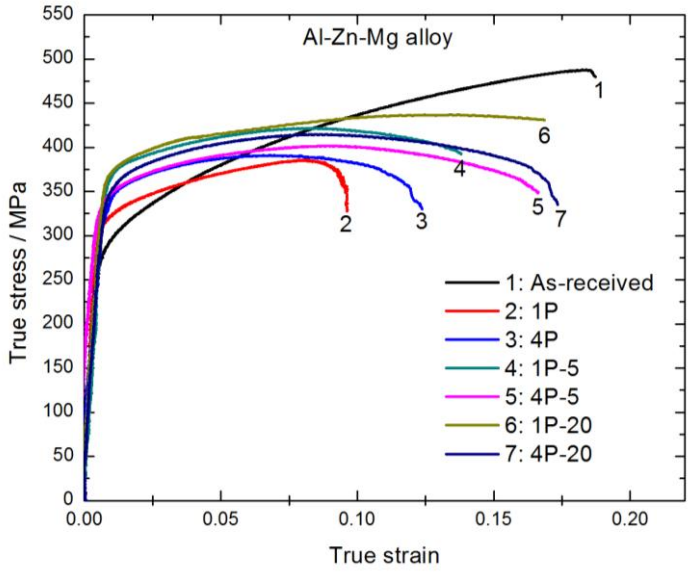

Fig. 1 True stress-true strain curves of the as-received Al-Zn-Mg alloy, ECAP processed at 423 K and post-ECAP heat treated at 393 K for 5 or 20 h.

Figure

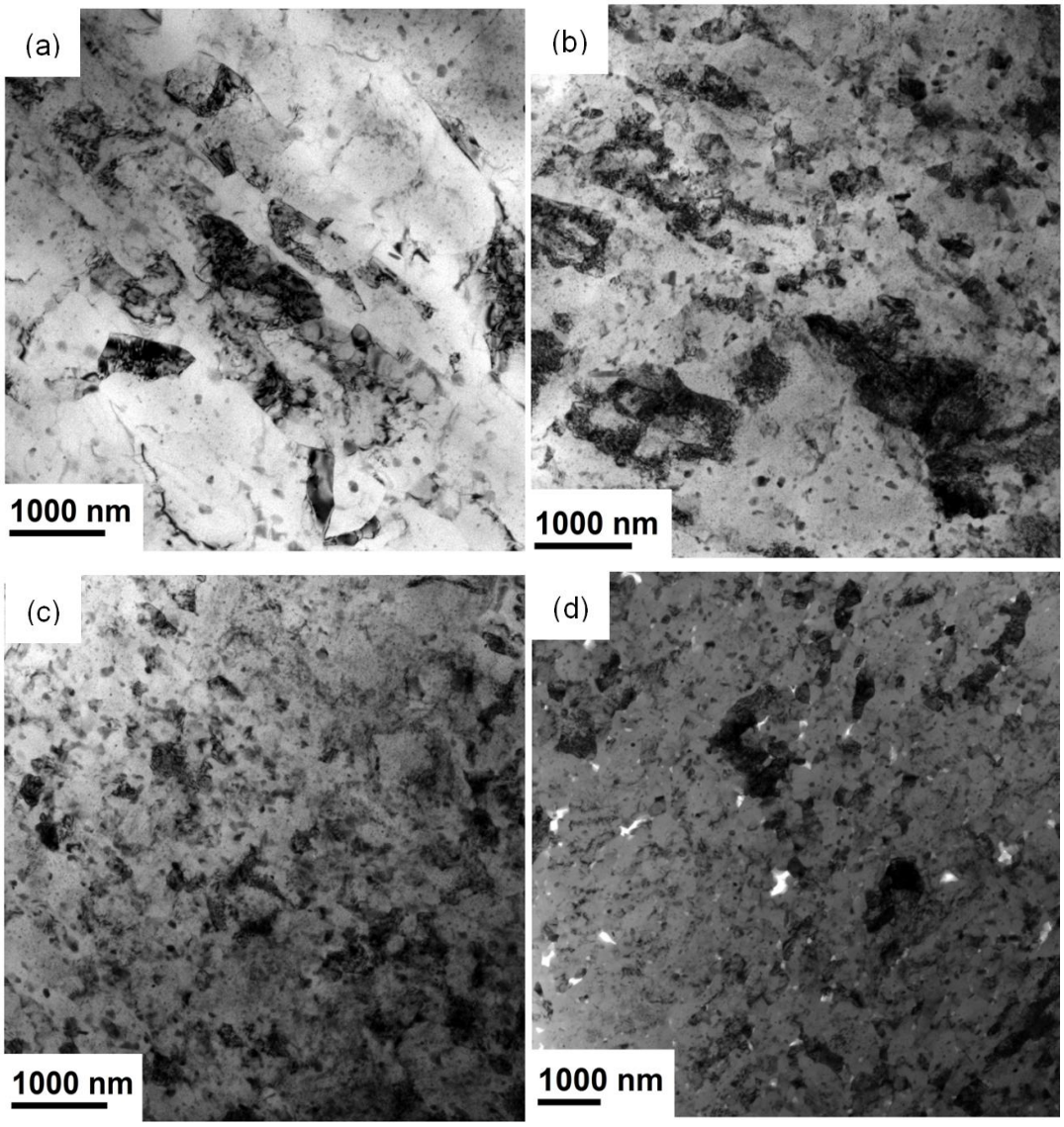

Fig. 2 Typical TEM micrographs of Al-Zn-Mg alloy along $<001>_{Al}$ zone axis processed by ECAP for 1 pass followed by heat treatments at 393 K for (a) 5 h, (b) 20 h, and by ECAP for 4 passes followed by heat treatments at 393 K for (c) 5 h and (d) 20 h.

Figure

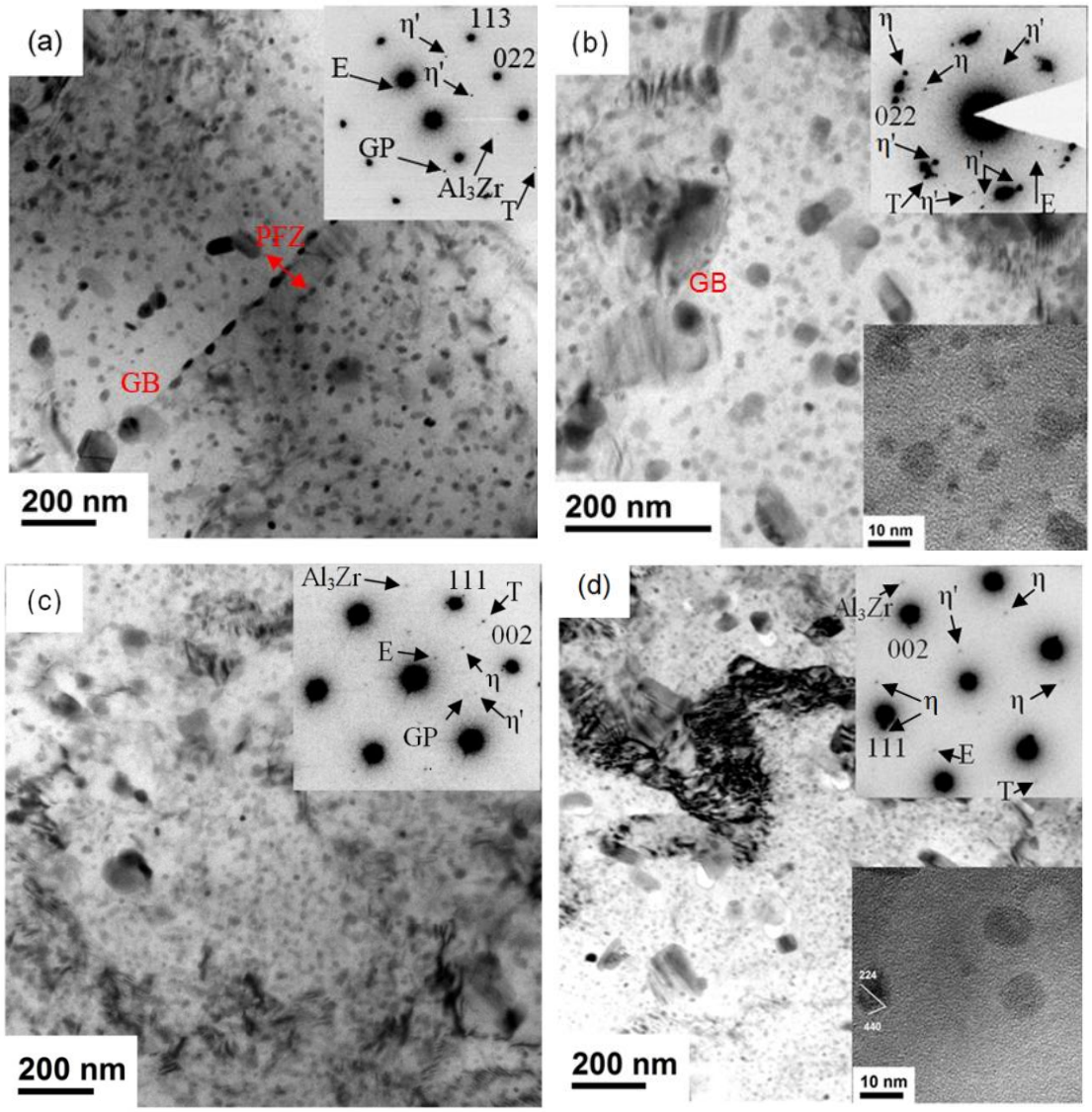

Fig. 3 Typical TEM micrographs and corresponding SAED of Al-Zn-Mg alloy processed by ECAP for 1 pass followed by heat treatment at 393 K for (a) 5 h, (b) 20 h, and by ECAP for 4 passes followed by heat treatment at 393 K for (c) 5 h and (d) 20 h.

Figure

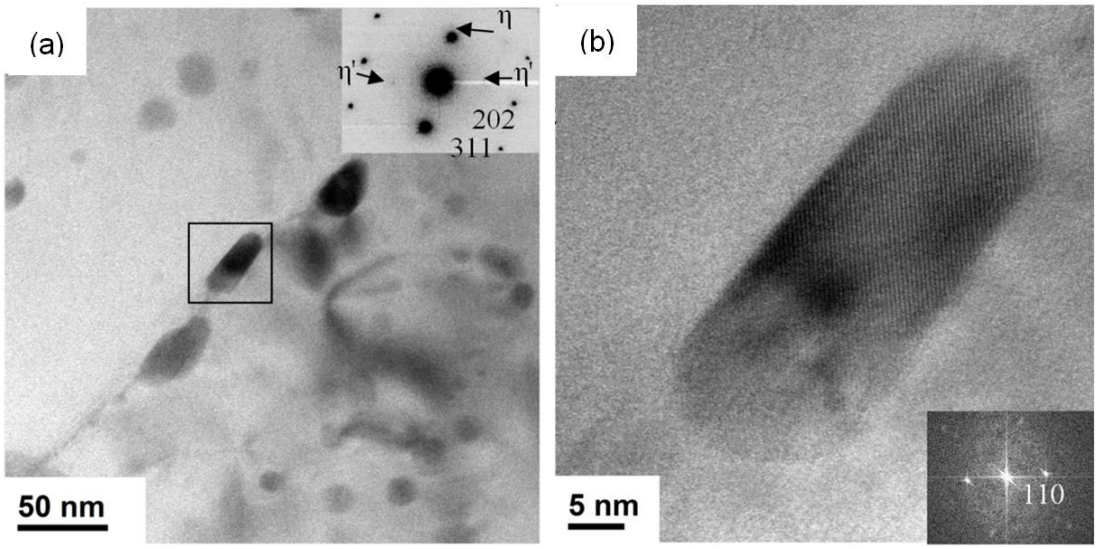

Fig. 4 TEM Micrographs of the Al-Zn-Mg alloy after ECAP for 1 pass and post-ECAP heat treatment at 393 K for 5 h: (a) TEM image showing PFZ and precipitates along the grain boundary with corresponding SAED along $<112>_{Al}$ and (b) HRTEM image of a plate-like η' phase along the grain boundaries.

Figure

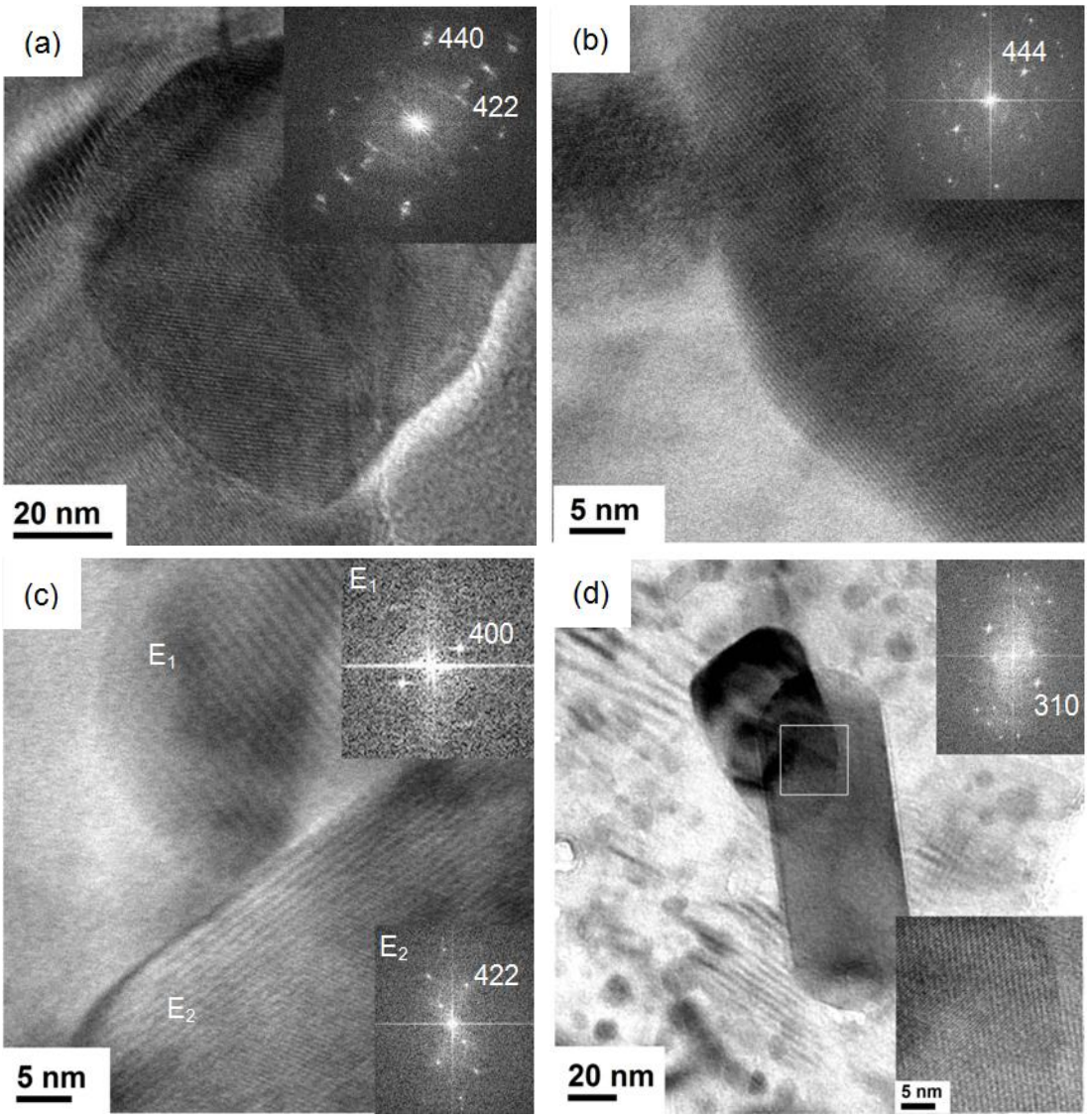

Fig. 5 HRTEM images of different phases in the Al-Zn-Mg alloy after ECAP for 1 pass followed by heat treatment at 393 K for 20 h showing overlapping of (a) two spherical E phases, (b) two spherical T phases, and after ECAP for 4 passes followed by heat treatment at 393 K for 20 h showing overlapping (c) one spherical with one platelet E phase and (d) two platelets T phases.